

Investigation of thermal transport in polymer composites with percolating networks of silver thin films by the flash diffusivity method

Sigurd R. Pettersen, Shijo Nagao, Helge Kristiansen, Susanne Helland, John Njagi, Katsuaki Suganuma, Zhiliang Zhang, and Jianying He

Citation: *Journal of Applied Physics* **121**, 025101 (2017); doi: 10.1063/1.4973682

View online: <https://doi.org/10.1063/1.4973682>

View Table of Contents: <http://aip.scitation.org/toc/jap/121/2>

Published by the [American Institute of Physics](#)

Articles you may be interested in

[Electromechanical characterization of individual micron-sized metal coated polymer particles](#)

Journal of Applied Physics **119**, 245102 (2016); 10.1063/1.4954218

[Self-healing of cracks in Ag joining layer for die-attachment in power devices](#)

Applied Physics Letters **109**, 093503 (2016); 10.1063/1.4962333

[Phonon transport at interfaces between different phases of silicon and germanium](#)

Journal of Applied Physics **121**, 025102 (2017); 10.1063/1.4973573

[Electrical four-point probing of spherical metallic thin films coated onto micron sized polymer particles](#)


Applied Physics Letters **109**, 043103 (2016); 10.1063/1.4959783

[A simple model of thermoelastic heat switches and heat transistors](#)

Journal of Applied Physics **121**, 024503 (2017); 10.1063/1.4974011

[Computational study of textured ferroelectric polycrystals: Dielectric and piezoelectric properties of template-matrix composites](#)

Journal of Applied Physics **121**, 024101 (2017); 10.1063/1.4973683



Instruments for Advanced Science

Contact Hiden Analytical for further details:
W www.HidenAnalytical.com
E info@hiden.co.uk

CLICK TO VIEW our product catalogue



Gas Analysis

- dynamic measurement of reaction gas streams
- catalysis and thermal analysis
- molecular beam studies
- dissolved species probes
- fermentation, environmental and ecological studies



Surface Science

- UHV TPD
- SIMS
- end point detection in ion beam etch
- elemental imaging - surface mapping



Plasma Diagnostics

- plasma source characterization
- etch and deposition process reaction kinetic studies
- analysis of neutral and radical species



Vacuum Analysis

- partial pressure measurement and control of process gases
- reactive sputter process control
- vacuum diagnostics
- vacuum coating process monitoring

Investigation of thermal transport in polymer composites with percolating networks of silver thin films by the flash diffusivity method

Sigurd R. Pettersen,^{1,a)} Shijo Nagao,² Helge Kristiansen,^{1,3} Susanne Helland,⁴ John Njagi,⁵ Katsuaki Suganuma,² Zhiliang Zhang,¹ and Jianying He^{1,b)}

¹*NTNU Nanomechanical Lab, Department of Structural Engineering, Norwegian University of Science and Technology (NTNU), NO-7491 Trondheim, Norway*

²*Institute of Scientific and Industrial Research (ISIR), Osaka University, Ibaraki, Osaka 567-0047, Japan*

³*Conpart AS, NO-2013 Skjetten, Norway*

⁴*Mosaic Solutions AS, NO-2013 Skjetten, Norway*

⁵*Center for Advanced Materials Processing, Clarkson University, Potsdam, New York 13699-5814, USA*

(Received 17 October 2016; accepted 22 December 2016; published online 9 January 2017)

The flash diffusivity method, also known as laser flash analysis (LFA), is commonly used to obtain the thermal diffusivity (α) and thermal conductivity (κ) of materials, due to its relative simplicity, rapid measurements, small sample size requirement, and standardized commercially available instruments. In this work, an epoxy adhesive was filled with a large fraction of homogeneous micron-sized polymethylmethacrylate spheres coated with thin silver films, such that a percolating metallic network that dominated the electric and thermal transport formed through the polymer at <3 vol. % silver. Specific heat capacity (C_p) was measured from the LFA measurements by a comparative method and from the total and reversible heat flow signals of modulated differential scanning calorimetry (MDSC). κ was estimated as the product of α , C_p , and density (ρ) and was found to vary significantly with the method to find C_p . The electron contribution was found from the electrical conductivity by the Wiedemann–Franz law and was used to elucidate the thermal transport mechanisms in the composite. A theoretical background for the various methods is included. Published by AIP Publishing. [<http://dx.doi.org/10.1063/1.4973682>]

I. INTRODUCTION

Thermal management becomes ever more important in electronic packaging, and increasing the thermal conductivity of packaging materials such as polymers is thus a high priority for the academic community and industry.^{1,2} To increase the thermal conductivity of polymer interconnect materials, thermally conductive fillers are typically added to the polymer matrix at high filler loadings (>30 vol. %).¹ Such fillers can be carbon-based (e.g., graphite, graphene, carbon black, carbon nanotubes, carbon fibers, or diamond) or ceramic or metal particles.^{1,2} Isotropic conductive adhesives (ICAs) are a special class of polymer-based interconnect materials, where electrically conductive filler particles form a percolating, isotropic network through a polymer adhesive.^{3,4} ICAs are alternatives to metallic solders and are especially suitable for interconnects that require low processing temperatures or are difficult to wet with solders. Silver is the metal with lowest electrical resistivity and highest thermal conductivity, $1.62 \times 10^{-6} \Omega \text{ cm}$ and 429 W/m K at 25°C , respectively.⁵ Although copper is cheaper and almost as good a conductor, it is more easily oxidized, and while copper oxide is an insulator, silver oxide is conductive.^{3,4} Due to its superior electrical properties, silver is therefore the preferred filler material in ICAs. Typical commercial

ICAs are composed of a thermoset epoxy binder with silver flakes embedded for electrical and thermal conductivity, sometimes in combination with solid silver particles. Commercial ICAs attain electrical conductivities (σ) around 10^4 S/cm and thermal conductivities (κ) around 3 W/(m K) at normal curing conditions, but require a high content of silver, around 85 weight percent (wt. %) or up to 40 volume percent (vol. %).⁶ In addition, the silver flakes tend to align with the shear flow direction during processing, which can lead to large anisotropies in the conductive properties.⁶ In recent years, homogeneously sized polymer spheres coated with thin films of silver (AgPS) have been shown as a viable alternative to silver flakes and solid silver particles in ICAs.^{7,8} AgPS-based ICAs are truly isotropic, and as the spherical silver films are much thinner than the diameter of the polymer cores, most of the AgPS will be polymer, and percolating networks can be formed at much lower silver contents than in conventional ICAs. AgPS-based ICAs have been shown to yield $\sigma > 1500 \text{ S/cm}$ at less than 3 vol. % silver,^{7,8} and the mechanisms controlling the electrical properties of these conductive composites are starting to be clarified.^{8–11} However, investigation of the thermal properties of AgPS-based ICAs have been sparse, and to our best knowledge, only one paper has been published on the subject to date.⁷ The mechanisms controlling the thermal transport of these ICAs are still largely unexplored.

Thermal conductivity is typically measured indirectly through the flash diffusivity method, also known as laser flash analysis (LFA), due to its relative simplicity, rapid measurements, small sample size requirements, as well as

^{a)}Parts of this work were done during an academic stay at Institute of Scientific and Industrial Research (ISIR), Osaka University, Ibaraki, Osaka 567-0047, Japan.

^{b)}Author to whom correspondence should be addressed. Electronic mail: jianying.he@ntnu.no

the availability of standardized, commercial instruments.¹² In the method, thermal diffusivity (α), specific heat capacity (C_p), and volume density (ρ) are measured separately, and κ is calculated through^{12–15}

$$\kappa = \alpha \cdot C_p \cdot \rho, \quad (1)$$

where all factors, including the thermal conductivity, are functions of the temperature of the material. LFA is commonly used to estimate κ for polymer composites with percolating networks of fillers, but often without revealing and discussing the intermediate factors α , C_p , and ρ .^{6,7,16–19} C_p is commonly measured either by a comparative method directly from the LFA results¹³ or separately by differential scanning calorimetry (DSC),^{20,21} whereas the potential deviations between the two methods are overlooked.

In this work, we investigate an epoxy matrix with AgPS at equal filler content but varying silver film thicknesses, yielding composites with silver content ranging from 0.7 to 2.9 vol. %. Thermal diffusivity is measured by LFA, whereas specific heat capacity is estimated by both LFA and modulated DSC (MDSC), where the latter can separate the reversible and non-reversible contributions to the specific heat capacity. Specific heat capacity, and further thermal conductivity, is found to be very dependent on the measurement procedure. We show that the thermal properties of the composites are dominated by the silver thin films, as these have much higher thermal conductivity than the polymer matrix and form a percolating network. In addition, the electron contribution to the thermal conductivity is estimated from electric 4-point measurements using the Wiedemann-Franz law.^{22,23} By comparing the results from electronic and thermal measurements, we reveal more about the thermal transport in the composites than what would be possible by thermal measurement alone. Sec. II summarizes the mechanisms behind thermal transport in solid materials, as well as gives readers basic insight on the methods used in this work.

II. THEORY AND METHODOLOGY

A. Thermal transport and Wiedemann-Franz law

Heat is conducted through a material by heat carriers, which in solids will be charge carriers (electrons and holes), and atomic lattice vibrations, the energy quanta known as phonons.² Polymers are generally electrical insulators; thus, there are no free charge carriers, and heat is transported by phonons. As phonons are scattered by defects and non-crystalline sections, the thermal conductivity of polymers is strongly affected by their crystallinity and can vary from around 0.2 W/(m K) for amorphous polymers such as polymethylmethacrylate (PMMA) to around 0.5 W/(m K) for highly crystalline polymers. Contrarily, κ in metals is generally assumed to be dominated by electron transport, and there is thus a close relationship between σ and κ , as described by the Wiedemann-Franz law^{22,23}

$$\frac{\kappa}{\sigma} = L \cdot T. \quad (2)$$

Here, T is the absolute temperature in Kelvin, and L is the Lorenz factor. The theoretical value of $L = (\pi^2/3)(k_B/e)^2 = 2.44 \times 10^{-8} \text{ V}^2/\text{K}^2$, where k_B is Boltzmann's constant and e is the elementary charge.²³ The electrical conductivity is normally obtained from the 4-point method, where electrical current is passed through the sample between two points and the voltage is measured by two intermediate probes.¹² σ is then obtained by multiplying the resultant resistance (R) with an analytically or numerically established factor that accounts for the finite geometry of the sample. If the phonon contribution is neglectable, κ can be expressed as^{19,23}

$$\kappa = \kappa_e + \kappa_{ph} = \sigma \cdot L \cdot T + \kappa_{ph}, \quad (3)$$

where κ_e and κ_{ph} are the electron and phonon contributions to the thermal conductivity, respectively.

B. Laser flash analysis (LFA)

Thermal conductivity, κ , is typically obtained indirectly by first finding thermal diffusivity, α , through the LFA method, where α is the speed at which a heat pulse diffuses through the material. As can be seen from Eq. (1), α is the ratio between κ and C_p times ρ . The definition of α in Eq. (1) is derived on the assumption of a homogeneous, isotropic material.^{24–27} Using the LFA method to measure α and further to obtain κ for composites therefore requires the implicit approximation of the composite as a hypothetical homogeneous material, where κ , α , C_p , and ρ are effective properties of this material.^{24–27} The LFA method is named after the procedure first proposed by Parker *et al.*, where a short pulse or flash of thermal energy is released by a laser or flash lamp towards a thin material specimen, where it is absorbed on the surface.¹³ Part of the thermal energy is conducted through the material to the backside of the sample, where the surface temperature (T) rise is measured as a function of time (t), typically by an infrared (IR) detector, yielding transient curves ($T(t)$). By preparing samples with much larger width or diameter than thickness, the non-axial heat flow is assumed negligible. With this assumption and adiabatic conditions, i.e., no heat-loss from the sample surfaces, the time (t_x) required for the backside temperature (T_x) to rise from a baseline to a fraction (x) of the maximum temperature (T_m) can be used to calculate α through

$$\alpha = \frac{k_x \cdot l^2}{t_x}, \quad (4)$$

where l is the sample thickness and $k_x = 1.38/\pi^2$ at $x = 0.5$, i.e., at the half-rise time.^{13–15} Perfect adiabatic transients are rarely achieved, and several models exist to correct for heat losses, such as the methods proposed by Cowan^{28,29} and Clark and Taylor.³⁰ In these methods, α at the half rise time as estimated from Eq. (4) is corrected by multiplication with $K_c/k_{0.5}$, where K_c is a correction factor dependent on the ratios of the rise times at certain points in the transients.¹⁴ In modern commercial LFA instruments, the methods are implemented by fitting the whole transients to the models by least-squares methods.³¹

The unknown C_p can be estimated from the same transients as α by comparison to a reference sample with known C_p values.^{13–15} The specific heat capacity (heat capacity per unit mass) is a measure for the amount of thermal energy (Q) required to increase the unit temperature per unit mass of a material by ΔT (in K or °C)

$$C_p = \frac{Q}{m \cdot \Delta T}. \quad (5)$$

If the heat source releases the same amount of thermal energy in each flash and the heat absorption of the reference and unknown sample is equal, Eq. (5) can be rewritten as $Q = (C_p \cdot m \cdot \Delta T)_{ref} = (C_p \cdot m \cdot \Delta T)_{sample}$, where ΔT is the temperature difference from the baseline to the maximum temperature ($T_m - T_b$). As $m = \rho \cdot V = \rho \cdot l \cdot A$, where l is the thickness of the sample and A is the surface area, this becomes $(C_p \cdot \rho \cdot l \cdot A \cdot \Delta T)_{ref} = (C_p \cdot \rho \cdot l \cdot A \cdot \Delta T)_{sample}$. If $A_{ref} = A_{sample}$, which can be solved by placing an aperture with a fixed opening between the flash lamp and samples, the unknown C_p of the sample can be found by

$$C_{p,sample} = \frac{(C_p \cdot \rho \cdot l \cdot \Delta T)_{ref}}{(\rho \cdot l \cdot \Delta T)_{sample}}. \quad (6)$$

When C_p is derived from LFA by the comparative method, the density of the unknown sample is a factor that must be measured and taken into account. However, it is easily seen by combining Eq. (6) with Eq. (1) that κ is independent of ρ_{sample} , i.e., that any arbitrary value can be used for the density of the sample if one is only interested in κ . Still, for Eq. (6) to be valid, in addition to the requirement of identical heat absorption, heat loss must be negligible or known in both the reference and unknown sample, which is all but impossible to achieve. The method is thus still prone to experimental errors and is often found to be unreliable and lead to underestimation of κ .¹²

C. Modulated differential scanning calorimetry (MDSC)

The most frequently used method for obtaining C_p is differential scanning calorimetry (DSC),¹² in which the difference in heat flow required to heat or cool the sample and an inert reference sample (often an empty crucible) at the same, controlled heating or cooling rate is measured.³² The differential heat flow signal can be used to identify phase changes such as melting of crystalline polymers (endothermic), kinetic processes such as epoxy curing (exothermic) and stress relaxation (endothermic), and material transitions such as the glass transition of amorphous polymers (endothermic).^{20,33} However, the signal will be a superposition of all individual contributions, and overlapping contributions can be difficult to separate and identify.³³ The total differential heat flow (dQ/dt) (W) can be described by the general equation³³

$$\frac{dQ}{dt} = C \cdot \frac{dT}{dt} + f(T, t), \quad (7)$$

where C is the heat capacity of the material (J/°C), dT/dt is the heating rate (°C/s), and $f(T, t)$ (W) is the heat flow from

kinetic processes, only dependent on time at an absolute temperature. In regular DSC, an (apparent) C_p can be calculated by comparing the total heat flow per unit mass of the sample to the heat flow per unit mass of a reference with known C_p .³² However, when the heating rate is constant, the heat capacity and kinetic components cannot be separated, and the calculated apparent C_p will contain both reversible (heat-capacity) and non-reversible (kinetic) components. Modulated DSC (MDSC) solves this by overlaying a modulated (most commonly sinusoidal) low-frequency perturbation onto the standard linear temperature ramp of a regular DSC scan.^{20,21,33} The reversible component of the apparent total heat capacity, $C_{p,rev}$, is then acquired directly from the ratio of the modulated heat flow amplitude to the modulated heating rate amplitude times the sample mass.²¹ The apparent, or total, $C_{p,tot}$ is calculated from the ratio of the normalized average heat flow to the underlying heating rate times the sample mass and should upon the fulfillment of certain experimental conditions equal the apparent C_p obtained from regular DSC. A more detailed review of the theory behind MDSC is given by Simon.²¹ According to ASTM standard E2716–09, the estimated C_p should be calibrated by multiplication with a specific heat capacity constant K_{Cp} , which is obtained by performing the same measurement on a sapphire control sample and taking the ratio between the known reference and measured C_p of the sapphire sample.³⁴ The last value, that of the non-reversible components, is then obtained by²¹

$$C_{p,non-rev} = C_{p,tot} - C_{p,rev}. \quad (8)$$

III. EXPERIMENTAL

A. Sample preparation

AgPS comprised of monodisperse PMMA spheres with a nominal diameter of 30 μm and four different nominal silver film thicknesses (60 nm, 100 nm, 150 nm, and 270 nm) were provided by Mosaic Solutions AS (Skjetten, Norway) and mixed into epoxy to create four ICA series. ICAs and epoxy control samples were molded as detached bricks with dimensions 10 mm \times 10 mm \times 1 mm and cured at 150 °C for 30 min. A summary of the pre-cure densities, AgPS content, and silver content of the five sample series can be observed in Table I. For more details on sample preparation, see Ref. 8.

To create clean and planar surfaces, six samples from each series were polished on both sides at 150 rpm using SiC paper from Struers (#4000; grain size 5 μm). Typical sample surfaces before and after polishing can be observed in Fig. 1.

The dimensions of each sample after polishing were measured at room temperature using a digital caliper with 1 μm resolution. The thickness of each sample was averaged from four measurements. The side lengths were measured, and the volume was calculated by assuming rectangular cuboid samples. Each sample was weighed using a balance with 0.1 mg resolution. The density at room temperature was calculated for each sample, and further averaged for each series.

TABLE I. Calculated pre-cure densities, volume fractions (vol. %), and weight fractions (wt. %) of the epoxy and four ICA series. Calculations are based on the weight fractions (measured) and nominal densities (given by the manufactures) of the constituents, as well as nominal diameter and film thicknesses of the AgPS.

Series	Nominal film thickness (nm)	Density (g/cm ³)	AgPS (vol. %)	AgPS (wt. %)	Silver (vol. %)	Silver (wt. %)
Epoxy	na	1.11	0.0%	0.0%	0.0%	0.0%
60Ag	60	1.20	55.7%	59.0%	0.7%	5.8%
100Ag	100	1.24	55.9%	60.5%	1.1%	9.3%
150Ag	150	1.29	56.3%	62.4%	1.7%	13.4%
270Ag	270	1.41	56.1%	65.5%	2.9%	21.7%

B. Electrical conductivity measurements

The electrical volume conductivity was measured directly on the polished surfaces of six samples from each ICA series using a 4-pin setup (Loresta-GP MCP-T610 with a 4-pin NSCP probe, Mitsubishi Chemical Analytech, Japan). The probe had inter-pin spacings of 1 mm, pinhead radii of 0.04 mm, and a spring pressure of 250 g/pin, ensuring equal contact pressure during each measurement. Four measurements were conducted on both sides of every sample, with the probe centered on the samples and the four pins parallel to the sample sides. The conductivity was calculated by

$$\sigma = \frac{1}{R \cdot l \cdot RCF}, \quad (9)$$

where R is the measured resistance, l is the thickness of the sample, and RCF is a resistivity correction factor calculated by the instrument to account for the positioning and pin spacing of the probe and the geometry of the samples. The Wiedemann-Franz law (Eq. (2)) was used to calculate the corresponding thermal conductivity, using the theoretical Lorenz factor ($2.44 \times 10^{-8} \text{ V}^2/\text{K}^2$) and $T = 298 \text{ K}$.

C. Laserflash analysis

α of the ICA and epoxy control series were determined by LFA at 25 °C, 50 °C, 75 °C, 100 °C, and 125 °C using a laserflash analysis instrument (LFA 447, Netzsch GmbH, Germany). The LFA and 4-pin measurements were performed on the same samples, but the electrical measurements were conducted before the ICA samples were prepared for the LFA measurements. The epoxy control samples were initially transparent and were therefore coated with approximately 120 nm gold on both sides using an ion sputter (E-1045, Hitachi, Japan) to eliminate transmission of light through the samples, as recommended by the ASTM

standard.¹⁴ All samples, including epoxy control and reference samples, were further spray coated with a thin layer of carbon on both sides to reduce reflectivity, maximize heat absorption, and ensure similar surface properties. Each sample was measured three times at each temperature, and α from each measurement was calculated with the instrument software (LFA Analysis, v. 4.8.3) using the Cowan model²⁹ with pulse correction.

An alumina reference sample with known C_p was measured under the same conditions as the ICA and epoxy samples. Each measurement on the ICA and epoxy samples was compared to the reference measurement using the instrument software (LFA Analysis, v. 4.8.3) to estimate the unknown C_p values.

D. Modulated differential scanning calorimetry

Samples were prepared by cutting small pellets from the detached ICA and epoxy bricks. To avoid the influence from the LFA heating on the thermal history of the samples, MDSC was not done on the same samples as the LFA and 4-pin measurements. The samples were polished to achieve a smooth surface and good thermal contact to the crucibles. The measurements were conducted with a differential scanning calorimeter (Q2000, TA Instruments, USA), starting with temperature equilibration at 0.00 °C for 10 min, followed by an average temperature increase of 2.00 °C/min with a modulation of $\pm 0.50 \text{ °C}$ per 100 s. Baseline measurements were performed with empty crucibles, and a sapphire reference sample was measured with the same parameters. An instrument calibration factor $K_{C_p}(T)$ was calculated as $C_{p,ref-table}(T)/C_{p,ref-measured}(T)$, where $C_{p,ref-table}(T)$ was taken from ASTM standard E1269–11.³² The C_p from each measurement on the ICA and epoxy samples was corrected by multiplication with $K_{C_p}(T)$.

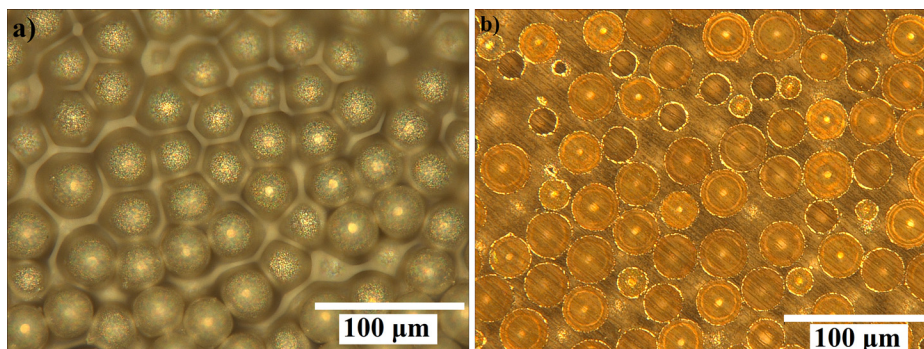


FIG. 1. Optical micrographs of the surface of a sample from the 270Ag series as-prepared (a) and after mechanical polishing (b).

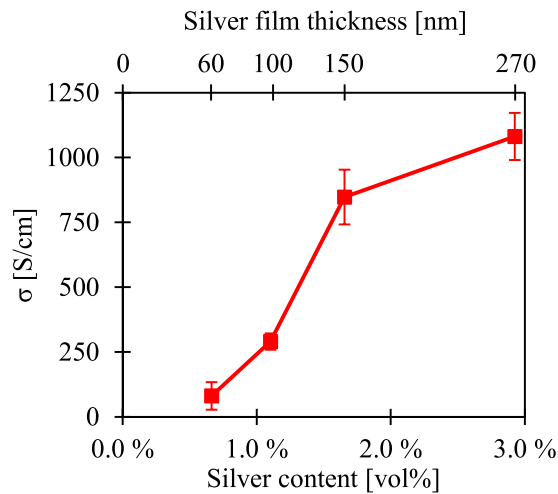


FIG. 2. Electrical conductivity of the four ICA series as a function of silver content. Error bars = \pm standard deviation.

The glass transition temperatures (T_g) of the epoxy and PMMA cores were estimated from the reversible $C_p(T)$ curves as the temperatures at half height of the transitions, using the software TA Instruments Universal Analysis 2000 (version 4.5 A build 4.5.0.5).

IV. RESULTS

A. Electrical conductivity

As seen in Fig. 2, the conductivity increases with increasing silver content, i.e., with thicker films. The variation from sample to sample is larger than variations between different measurements on the same sample and is the main cause behind the observed scatter.

B. Thermal diffusivity

Fig. 3 shows the thermal diffusivity of the epoxy and ICA series as a function of temperature. The diffusivity is highly dependent on the silver content. As seen in Table I, the silver content of the 60Ag series is estimated to be only 0.7 vol. %, but already with this small amount of silver, the diffusivity shows a relative increase of 183% at 25°C

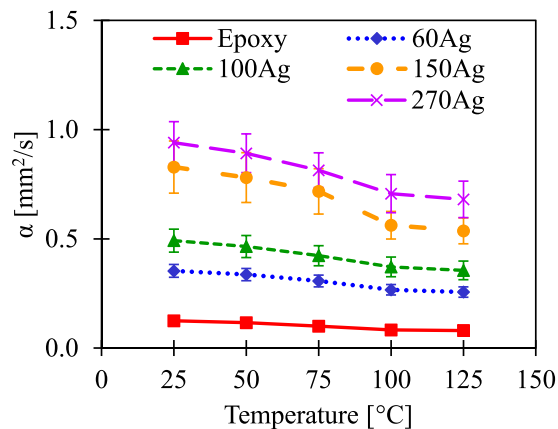


FIG. 3. Thermal diffusivity of the four ICA and epoxy control series. Error bars = \pm standard deviation.

compared to pure epoxy. As with the 4-pin measurements, the deviations are caused by sample variation. The three measurements on each sample at each temperature always yielded close to equal values.

C. Glass transitions and specific heat capacity

Fig. 4(a) shows that the reversible C_p values of the epoxy and ICA series decrease with increasing silver content. The ICAs reveal two clear glass transitions, one at around 65°C and another at approx. 122.5°C. The epoxy sample only goes through the first transition, suggesting that the second transition in the ICAs is that of the PMMA cores.

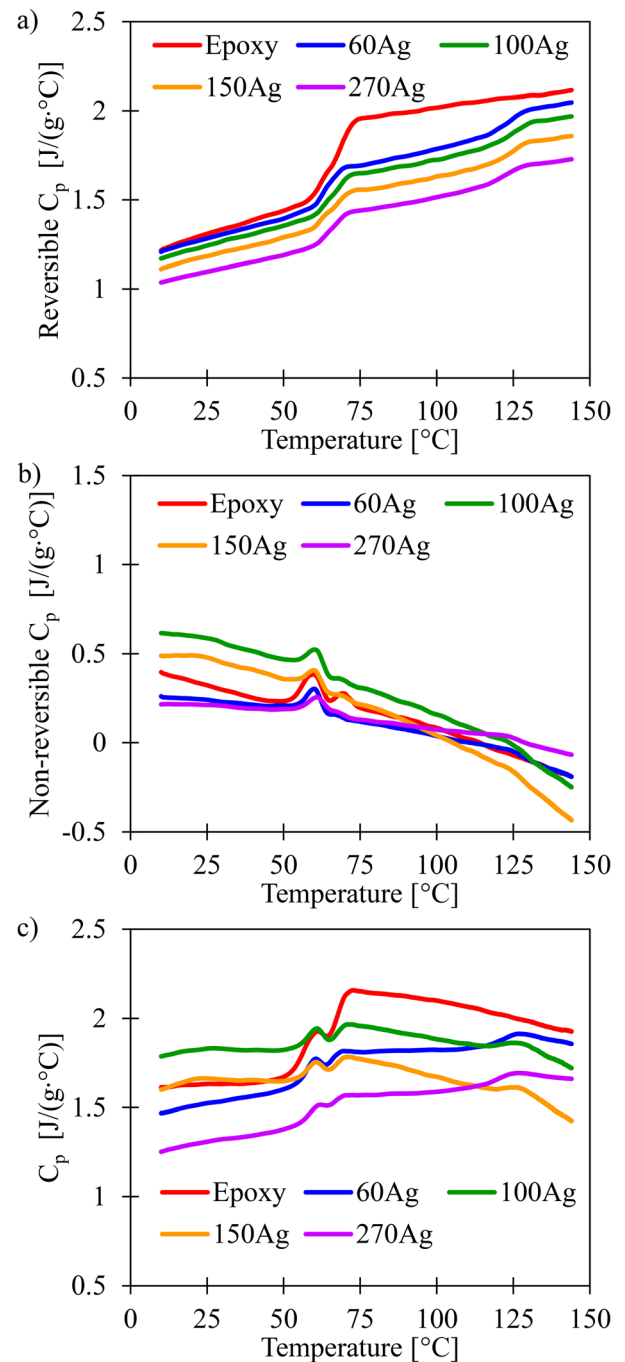


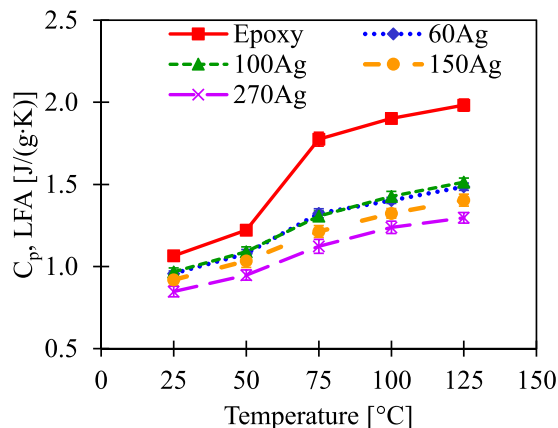
FIG. 4. Reversible (a), non-reversible (b), and total (c) specific heat capacity of the four ICA and epoxy control series.

TABLE II. Glass transition temperatures (T_g) of the epoxy of the four ICA and epoxy control series, as well as for the PMMA cores in the ICAs.

Series	$T_{g,epoxy}$ ($^{\circ}\text{C}$)	$T_{g,PMMA}$ ($^{\circ}\text{C}$)
Epoxy	66.8	na
60Ag	63.5	122.9
100Ag	66.5	122.9
150Ag	64.4	122.9
270Ag	64.9	121.2
Average	65.2	122.5
Standard deviation	1.4	0.8

T_g for each series can be found in Table II. Although the reversible C_p increases with temperature, with steps at the glass transitions, the non-reversible C_p (Fig. 4(b)) shows the opposite behavior, decreasing with temperature, crossing from endothermic to exothermic in the interval between 100 and 125 $^{\circ}\text{C}$. The non-reversible C_p curves also reveal an endothermic process that peaks approximately where the glass transition starts to occur. During a second measurement on the 150Ag sample, this peak is no longer present (see [supplementary material](#)), suggesting that this peak may be caused by release of residual stress from, e.g., the sample polishing or curing process as the epoxy goes from a rigid to flexible structure during the first MDSC heating.

These endothermic relaxation peaks are also present in the total C_p signal (Fig. 4(c)). However, as they occur in the range between 50 and 75 $^{\circ}\text{C}$, they do not affect the values at the relevant temperatures (25, 50, 75, 100, and 125 $^{\circ}\text{C}$). Still, there is an increase in the total C_p from 50 to 75 $^{\circ}\text{C}$ in all the samples, caused by the glass transition of the epoxy. Total C_p decreases for the epoxy, 100Ag, and 150Ag series after 75 $^{\circ}\text{C}$, as the non-reversible C_p dominates the reversible C_p for these samples at elevated temperatures. In addition, the non-reversible C_p signals do not show the same dependence on silver content as the reversible signals, a result that is reflected in the total C_p signal from the MDSC measurement. On the other hand, the C_p from LFA correlates much better with the silver content, and the similarity with the reversible C_p signal from the MDSC measurements is conspicuous. As seen in Fig. 5, the LFA method captures the glass transition of the epoxy, although the second transition, presumably that

FIG. 5. Specific heat capacity from LFA. Error bars = \pm standard deviation.

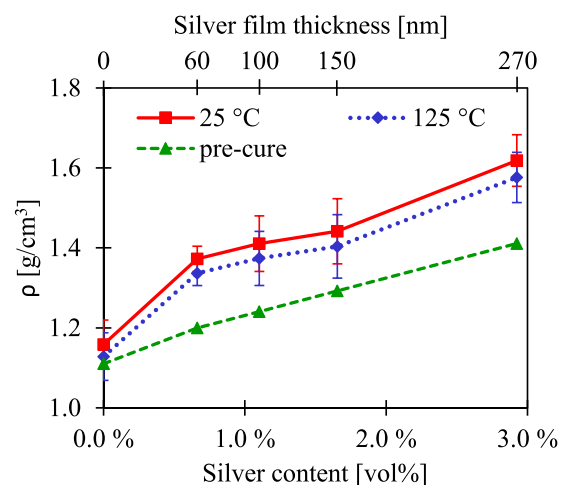
of the PMMA cores, is not visible. LFA also yields somewhat lower C_p values than MDSC.

D. Density

Fig. 6 compares the densities of the epoxy and ICA series before and after cure. The estimated density increases after cure, which is expected due to shrinkage of the epoxy matrix caused by cross-linking during the curing process. The estimated density also increases with increasing silver content, which is also natural, as silver (10.5 g/cm^3 at 25 $^{\circ}\text{C}$ (Ref. 5)) is about nine times more dense than the pre-cure epoxy, based on the data sheet values from the manufacturer. However, the density increases much more for the ICA than the epoxy, suggesting that the nominal densities of the AgPS may be too low. The values at 125 $^{\circ}\text{C}$ are calculated based on linear coefficients of thermal expansion (CTE) reported by Gakkestad *et al.*⁷ for an ICA with the same epoxy system and PMMA cores, although slightly lower AgPS content (46 vol. %). With these values, thermal expansion only leads to a relative increase of 0.89% in height and width of the samples from 25 $^{\circ}\text{C}$ to 125 $^{\circ}\text{C}$. The density dependence on CTE is three times larger, but the relative change is thus still only -2.62% , which is smaller than the standard deviations caused by sample variation at 25 $^{\circ}\text{C}$, as can be observed in Fig. 6. As there is some uncertainty in the transferability of the CTE values from Ref. 7 due to a higher AgPS-content in the ICAs in this work, thermal diffusivities and conductivities at elevated temperatures are estimated with the thickness and density values at 25 $^{\circ}\text{C}$.

E. Thermal conductivity

Thermal conductivity increases with silver content, as evident from Figs. 7 and 8. MDSC yields higher C_p than LFA, and with the same ρ and α , Eq. (1) thus yields the highest thermal conductivity with C_p from MDSC. $\kappa_{(C_p,LFA)}$ increases slightly to a peak at 75 $^{\circ}\text{C}$, which is caused by the glass transition of the epoxy in the interval between 50 $^{\circ}\text{C}$ and 75 $^{\circ}\text{C}$. At 100 $^{\circ}\text{C}$ and 125 $^{\circ}\text{C}$, the further increase in C_p is canceled by the decrease in α . For $\kappa_{(rev-C_p,MDSC)}$, the

FIG. 6. Densities of the four ICA and epoxy control series as a function of silver content. Error bars = \pm standard deviation.

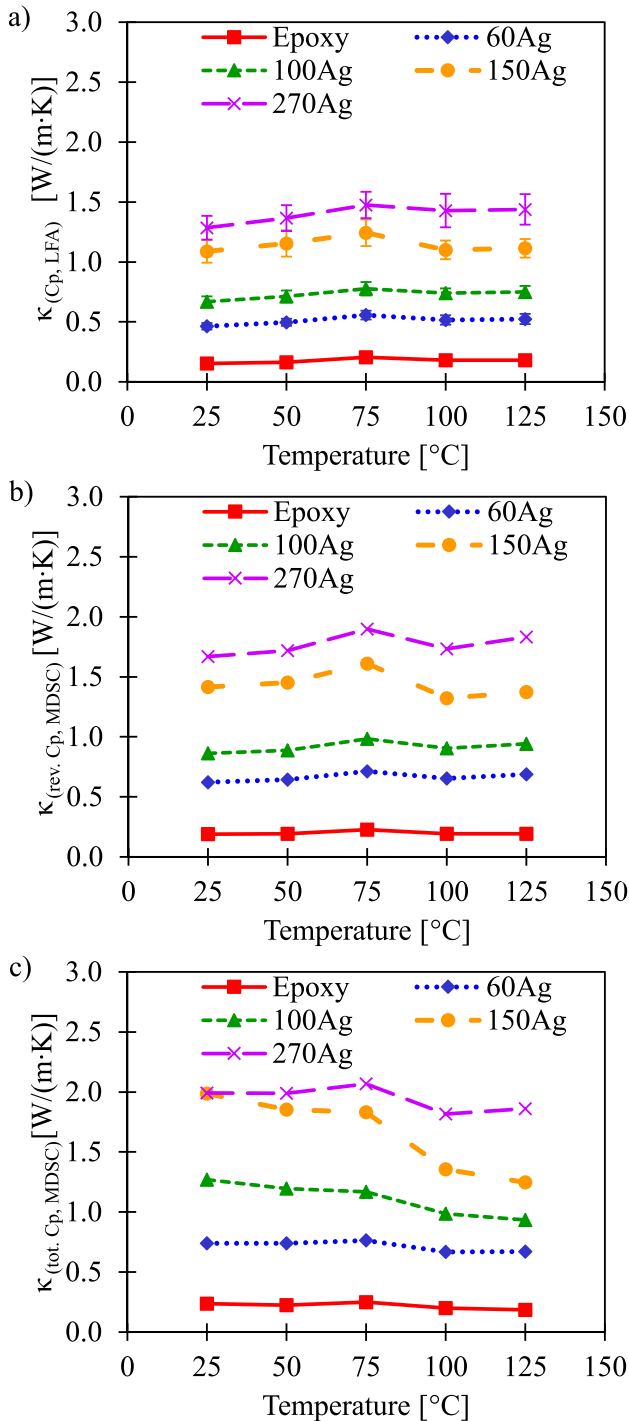


FIG. 7. Thermal conductivities of the four ICA and epoxy control series calculated using Eq. (1), with specific heat capacity (C_p) from LFA (a), reversible C_p from MDSC (b), and total C_p from MDSC (c).

behavior is similar to that of $\kappa(C_{p,LFA})$, but with a slight increase at 125°C caused by the glass transition of the PMMA cores, not observable in the LFA results. $\kappa(\kappa_{tot-Cp,MDSC})$ is affected by the more chaotic total C_p values, caused by the non-reversible part of the MDSC signal. This leads to $\kappa(\kappa_{tot-Cp,MDSC})$ being identical, 1.99 W/(m K) for both the 150Ag and 270 Ag series at 25°C. $\kappa(\kappa_{tot-Cp,MDSC})$ thus increases drastically with silver content, before leveling out before the series with thickest silver films on the AgPS, as observable in Fig. 8. This behavior is different from

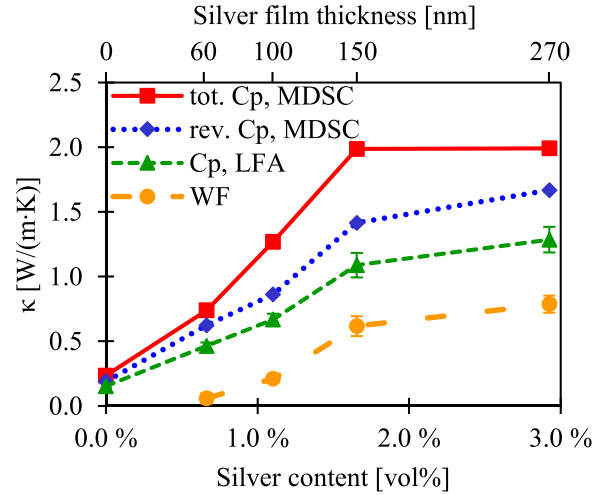


FIG. 8. Thermal conductivities of the four ICA and epoxy control series at 25°C, calculated using Eq. (1), with total C_p from MDSC, reversible C_p from MDSC, C_p from LFA, or from the electrical conductivity using the Wiedemann-Franz law (Eq. (2)).

$\kappa(\kappa_{rev-Cp,MDSC})$, $\kappa(C_{p,LFA})$, and $\kappa(\kappa_{WF})$, found from the electrical conductivity through the Wiedemann-Franz law (Eq. (2)). The trends from these methods are very similar, with κ increasing with silver content up to the 270Ag series, although with a lower gradient from the 150Ag and 270Ag series than from the epoxy/60Ag series to the 150Ag series. At 25°C, there is an upward shift of 0.40, 0.46, 0.47, and 0.50 W/(m K) between $\kappa(\kappa_{WF})$ and $\kappa(C_{p,LFA})$ for the 60Ag, 100Ag, 150Ag, and 270Ag series, respectively. From $\kappa(\kappa_{WF})$ to $\kappa(\kappa_{rev-Cp,MDSC})$, the upward shift is 0.56, 0.65, 0.80, and 0.88 W/(m K), respectively. These values are all larger than κ of the epoxy at 25°C, which is 0.15, 0.19, and 0.24 W/(m K) for $\kappa(C_{p,LFA})$, $\kappa(\kappa_{rev-Cp,MDSC})$, and $\kappa(\kappa_{tot-Cp,MDSC})$, respectively.

V. DISCUSSION

A. Percolating silver network

The electrical conductivity of AgPS-based ICAs has been extensively investigated elsewhere, but the main findings are repeated here for the convenience of the reader. Although the conductivity of these composites is a complex phenomenon, it will generally increase with increasing volume fraction of AgPS after reaching the percolation threshold of around 30–35 vol.%.¹¹ Below the percolation threshold, the filler concentration is too low for percolating conductive pathways to be formed. Above the percolation threshold, for the same volume fraction of AgPS, smaller particles^{7,11} and thicker films^{8,11} yield higher ICA conductivity. However, there are also factors that have a negative impact on the bulk ICA conductivity. It has been shown that the intrinsic conductivities of the spherical silver thin films are lower than that of bulk silver.¹⁰ This is mainly caused by increased electron scattering at grain boundaries as the grains become smaller than the electron mean free path of bulk silver, as well as possible impurities from the electroless plating process used to coat the polymer spheres with the silver thin films, and can even result in thicker films exhibiting lower intrinsic conductivities than thinner films.¹⁰ The silver

films on the AgPS of the 270Ag series have been shown to contain smaller grains than the series with less silver and thinner films,⁸ which explains why the conductivity levels out when reaching the highest silver content, as seen in Fig. 2. In addition to lower intrinsic conductivities, the spherical shell geometry will induce a geometrical constriction resistance that would not be present in a conductive filler with a constant cross-sectional area, although this constriction resistance will decrease with increasing interparticle contact radii.^{8,11} At ~ 56 vol. %, the AgPS are above the loose packing limit of randomly dispersed spheres (~ 53.6 vol. %), and not very far from the maximum random packing limit of ~ 63.4 vol. %.³⁵ This suggests that most AgPS participate in the conductive network, with the condition that they are able to form electrical contacts with the adjacent AgPS. It has been shown that the silver films of AgPS penetrate the epoxy and form continuous metallic inter-particle contacts after curing of the ICAs.^{8,9} Although electrons in theory can pass across very thin (< 10 nm) non-conductive barriers by quantum tunneling, this current will be negligible compared to a metallic contact of the same size.³⁶ The formation of metallic contacts helps explain why AgPS-based ICAs yield higher electrical conductivities relative to their silver content when compared with most conventional ICAs.⁸

It is evident that the electrical conductivity (Fig. 2), thermal diffusivity (Fig. 3), and thermal conductivity (Figs. 7 and 8) are dominated by the network of silver films, as these parameters all increase by several hundred percent upon the addition of only a few percent silver and increase with increasing silver content, i.e., thicker silver films. However, when the electron contribution to the effective thermal conductivity of the ICA is calculated from the Wiedemann-Franz law (2), the values are lower than κ from LFA and MDSC, as shown in Fig. 8. According to Eq. (3), this upward shift from $\kappa_{(WF)}$ is the phonon contribution to the effective thermal conductivity, which comes primarily from the epoxy matrix and PMMA cores. Although the silver films conduct a significant portion of the heat compared to their low volume fraction, the phonon contribution from the epoxy and PMMA cores still comprises a substantial part of the total effective thermal conductivity of the ICA. As already discussed, the transport of electrons is limited to occur within the silver films or by tunneling across very thin layers of polymer. Conversely, heat transport is not limited to the metal and can occur across the epoxy between adjacent silver films by phonon transport long before the films are close enough for electrons to be conducted across. A coupling between the electron transport of the silver films and the phonon transport of the polymer could help explain why the effective thermal conductivities of the ICAs are higher than the sum of the electron contribution and the thermal conductivity of the epoxy. The mechanisms of such heat transfer across the interface between the metal thin films and the polymer phases would be an interesting topic for further investigations.

An important prerequisite for the LFA method and indeed for the very definition of thermal diffusivity in Eq. (1) is that the sample can be regarded as a homogeneous material on the scale of the measurements.^{24–27} If the

transient heat wave was to be transported more rapidly through the percolating network of silver than through the polymer phases, the assumption of effective homogeneity would break down. α of bulk silver is $161 \text{ mm}^2/\text{s}$ at 22°C ,¹³ whereas the estimated α of the epoxy control samples is $0.125 \text{ mm}^2/\text{s}$ at 25°C . α of the ICAs ranges from 0.353 to $0.940 \text{ mm}^2/\text{s}$ at 25°C , much closer to that of epoxy than bulk silver, suggesting that the diffusion time is not dominated by the silver. As already discussed, the electrons of the silver conduct a significant portion of the heat. If this heat was to be conducted much more quickly than the heat conducted by the phonons of the polymer phases, we would expect to see an unusually sharp rise at the beginning of the transient $T(t)$ curves from the LFA measurements, and large deviations in the shape of the curves when compared with curves of a homogeneous material. However, the shapes of rising sections of the ICA curves are similar to the shape of the curves of the homogeneous epoxy control samples when normalized for the decreasing time scale of the measurements with increasing silver content. The heat loss decreases, i.e., the transient curves show a closer to adiabatic behavior, as the silver content increases, but this is presumably due to less radiation losses from the samples surfaces because of the shorter measurement times. Examples of transient curves for the epoxy and four ICA series can be seen in Figs. S1–S5 in the [supplementary material](#).

B. Deviations in results between different methods

It is obvious from Figs. 7 and 8 that both the absolute values and temperature-dependence of κ are highly dependent on the method chosen to obtain C_p . LFA is able to capture the T_g of the epoxy, but not the later T_g of the PMMA cores, and this method also yields the lowest C_p . As given by Eq. (7), reversible C_p is the true heat capacity of the composite, and as can be seen in Fig. 4(a), it is dependent on the relative amounts of the individual components. Silver has lower C_p ($0.235 \text{ J}/(\text{g } ^\circ\text{C})$ at 25°C (Ref. 5)) than epoxy, and it is expected that the C_p of the ICA decreases as the silver content increases, as observed in Fig. 4(a). The total C_p is a superposition of the reversible C_p and non-reversible C_p (kinetic processes), and as long as the sum of the kinetic processes are endothermic, the total C_p will be larger than the reversible C_p . As observed in Fig. 4(b), the non-reversible C_p becomes exothermic for the measured samples in the interval between 100 and 125°C . As a result, the total C_p , and further κ calculated from these values, is approximately equal or lower than the reversible C_p and the corresponding κ at 125°C , although these are lower at lower temperatures. The C_p found by regular DSC is, with some exceptions, the same as the total C_p found by MDSC,²¹ and as shown here, these values will be significantly affected by the thermal history of the samples. Great care and consideration should thus be taken when choosing the method for finding C_p .

An advantage in using MDSC is that the glass transitions of the composite can be identified from the reversible signal. It is obvious from Fig. 4(c) that identifying T_g from the chaotic signals for the total C_p is difficult. LFA yields similar curves as the reversible MDSC signal, but can only

give values at discrete temperatures, contrary to the continuous monitoring of the differential scanning method. The thermal conductivity of amorphous polymers increases with increasing temperature until T_g is reached,¹ upon which the polymer transitions from a hard and brittle glassy state to a soft and flexible rubbery state. Above the T_g , the thermal conductivity decreases with increasing temperature.¹ However, κ is a function of C_p , and as evident from both Figs. 4(a) and 5, C_p increases with a smooth step as the temperature exceeds the T_g of the polymer. According to Eq. (1), κ would only decrease above T_g if the increase in C_p is balanced and outweighed by a decrease in α and ρ . In Fig. 7, it is seen that κ generally increases up to 75 °C, and then decreases as the temperature is elevated further. The T_g of the epoxy is estimated to be around 65 °C, and from Fig. 4(a) it is clear that the transition is finished at 75 °C. However, as κ is not measured at 65 °C, it is possible that κ peaks at a slightly lower temperature than what is suggested in Fig. 7. As the reversible C_p from MDSC are the only values that increase with an extra step at the glass transition of the PMMA cores, κ only increases at 125 °C when these values are used. In the total C_p from MDSC, the increase in reversible C_p above the T_g of the PMMA cores is outweighed by the decrease in non-reversible C_p . The reason why the second T_g is not observable in the LFA results is possibly an outcome of the transiency of the method. Before each laser flash measurement, the temperature in the measurement chamber is equilibrated at the value of interest, and at 125 °C, the PMMA cores should have passed the half-way point of their glass transition. However, the T_g of ~ 122.5 °C is obtained from MDSC, with much slower perturbations (tens of seconds) than the transient laser flash (milliseconds). It is well known that the glass transition temperature is dependent on the heating rate of the measurement, with increasing heating rates yielding higher T_g .³⁷ Thus, we expect that increasing the chamber temperature above 125 °C would have revealed the glass transition of the PMMA cores also for the LFA measurements.

C. Thickness measurements

As seen in this work, uncertainties in the specific heat capacity can cause significant scatter in the thermal conductivity. The largest source of errors in the LFA procedure except for the specific heat capacity is variations in the measured thickness (l).¹² According to the equation for propagation of errors in expressions with a power law dependence, e.g., $\alpha = l^n$, the relative error $\Delta l/l$ will lead to a relative error $\Delta\alpha/\alpha$ by the relation³⁸

$$\frac{\Delta\alpha}{|\alpha|} = |n| \cdot \frac{\Delta l}{|l|}. \quad (10)$$

From the Parker expression (Eq. (4)), we get $\alpha \propto l^2$.¹³ The correction factors from the Cowan model^{28,29} and the Clark and Taylor model³⁰ are not dependent on l ,¹⁴ so thermal diffusivity is still dependent on the square of the thickness even if these commonly used heat loss corrections are employed. A relative error in the thickness measurements will thus lead

to twice the relative error in the thermal diffusivity. In (M)DSC, the input factor is the mass of the samples, and measurement errors in thickness will not affect C_p . For C_p estimated from LFA (Eq. (6)), we have that $C_p \propto (\rho \cdot l)^{-1}$. For a cylindrical or cuboid sample, $\rho \propto l^{-1}$, and C_p is thus independent of l when estimated from LFA. However, as discussed in Section II B, if C_p is measured by LFA, the ρ^{-1} dependence of C_p cancels against the ρ dependence of κ , when κ is estimated by Eq. (1). Thus, regardless of whether C_p is measured by (M)DSC or LFA, the thickness dependence of $\rho \cdot C_p \propto l^{-1}$. When κ is estimated by Eq. (1), there is a thickness dependence of $\kappa = \alpha \cdot \rho \cdot C_p \propto l^2 \cdot l^{-1} \propto l$. A relative error in the thickness measurements will directly lead to an equivalent relative error in the thermal conductivity.

VI. CONCLUSIONS

The thermal properties of ICA composites with silver coated polymer spheres forming a percolating metallic network throughout the polymer were investigated by MDSC and the commonly used flash diffusivity method. The thermal diffusivity increased by several hundred percent upon the addition of the filler particles but was still much closer to that of the epoxy matrix than that of bulk silver. The thermal conductivity was very sensitive to the method chosen to obtain C_p . The LFA method provided the easiest measurements, but yielded the lowest C_p and did not capture the glass transition of the polymer cores. The reversible signal from MDSC showed strong correlation with silver content, and the glass transitions of both the epoxy and polymer cores were easily distinguished. The total MDSC signal was more dependent on the thermal history of the samples and provided chaotic signals that did not necessarily correlate with silver content. Finally, the thermal conductivity was estimated from the electric conductivity by the Wiedemann-Franz law and was found to be smaller than the thermal conductivity found by the LFA method, although with similar dependence on silver content as the thermal conductivity with C_p from LFA or reversible C_p from MDSC. It was concluded that a large contribution to the effective thermal conductivity comes from electron conduction through the percolating network of silver films. However, there is also a significant contribution from phonon transport in the polymer phases.

SUPPLEMENTARY MATERIAL

See [supplementary material](#) for examples of transient LFA curves as well as MDSC data for the individual samples.

ACKNOWLEDGMENTS

The Research Council of Norway provided funding through Project No. 225962—“Novel Conductive Adhesive Technology for Solar Industry” and through Project No. 251068—“Engineering Metal-Polymer Interface for Enhanced Heat Transfer.” Partial funding has also been obtained from the European Commission programme FP7-NMP-2013-LARGE-7 under Grant Agreement No. 604668—“Quantheat.” S. R. Pettersen appreciates financial support

given by Osaka University through the Frontier Mini Program and from the Norwegian Ph.D. Network on Nanotechnology for Microsystems, which is sponsored by the Research Council of Norway, Division for Science, under Contract No. 221860/F40. The authors are grateful to Ignat Tolstorebrov (Department of Energy and Process Engineering, NTNU) for his skillful conductance of the MDSC measurements.

- ¹Z. Han and A. Fina, *Prog. Polym. Sci.* **36**, 914 (2011).
- ²A. L. Moore and L. Shi, *Mater. Today* **17**, 163 (2014).
- ³M. J. Yim, Y. Li, K.-S. Moon, K. W. Paik, and C. P. Wong, *J. Adhes. Sci. Technol.* **22**, 1593 (2008).
- ⁴J. E. Morris and J. Liu, in *Micro- and Opto-Electronic Materials and Structures: Physics, Mechanics, Design, Reliability, Packaging*, edited by E. Suhir, Y. C. Lee, and C. P. Wong (Springer Science+Business Media LLC, New York, 2007), p. 527.
- ⁵D. R. Lide, *CRC Handbook of Chemistry and Physics*, 84th ed. (Taylor & Francis, 2003).
- ⁶M. Inoue, H. Muta, T. Maekawa, S. Yamanaka, and K. Suganuma, *J. Electron. Mater.* **38**, 430 (2009).
- ⁷J. Gakkestad, L. Zhuo, T. Helland, and C. P. Wong, *IEEE 15th Electronics Packaging Technology Conference (EPTC)* (Singapore, 2013), p. 213.
- ⁸S. R. Pettersen, H. Kristiansen, S. Nagao, S. Helland, J. Njagi, K. Suganuma, Z. Zhang, and J. He, *J. Electron. Mater.* **45**, 3734 (2016).
- ⁹S. R. Pettersen, H. Kristiansen, K. Redford, S. Helland, E. Kalland, Z. Zhang, and J. He, *IEEE 66th Electronic Components and Technology Conference (ECTC)* (2016), p. 2494.
- ¹⁰S. R. Pettersen, A. E. Stokkeland, H. Kristiansen, J. Njagi, K. Redford, D. V. Goia, Z. Zhang, and J. He, *Appl. Phys. Lett.* **109**, 043103 (2016).
- ¹¹S. Jain, Ph.D. thesis, Loughborough University, UK, 2016.
- ¹²K. A. Borup, J. De Boor, H. Wang, F. Drymiotis, F. Gascoin, X. Shi, L. Chen, M. I. Fedorov, E. Müller, and B. B. Iversen, *Energy Environ. Sci.* **8**, 423 (2015).
- ¹³W. J. Parker, R. J. Jenkins, C. P. Butler, and G. L. Abbott, *J. Appl. Phys.* **32**, 1679 (1961).
- ¹⁴ASTM E1461-13, *Standard Test Method for Thermal Diffusivity by the Flash Method* (ASTM International, West Conshohocken, PA, USA, 2013).
- ¹⁵W. Nunes dos Santos, P. Mummery, and A. Wallwork, *Polym. Test.* **24**, 628 (2005).
- ¹⁶S. Ganguli, A. K. Roy, and D. P. Anderson, *Carbon* **46**, 806 (2008).
- ¹⁷W. S. Lee and J. Yu, *Diamond Relat. Mater.* **14**, 1647 (2005).
- ¹⁸S. Yu, J.-W. Lee, T. H. Han, C. Park, Y. Kwon, S. M. Hong, and C. M. Koo, *ACS Appl. Mater. Interfaces* **5**, 11618 (2013).
- ¹⁹K. Zhang, Y. Zhang, and S. Wang, *Carbon* **65**, 105 (2013).
- ²⁰P. S. Gill, S. R. Sauerbrunn, and M. Reading, *J. Therm. Anal.* **40**, 931 (1993).
- ²¹S. L. Simon, *Thermochim. Acta* **374**, 55 (2001).
- ²²G. V. Chester and A. Thellung, *Proc. Phys. Soc.* **77**, 1005 (1961).
- ²³N. Stojanovic, D. Maithripala, J. Berg, and M. Holtz, *Phys. Rev. B* **82**, 075418 (2010).
- ²⁴J. F. Kerrisk, *J. Appl. Phys.* **42**, 267 (1971).
- ²⁵J. F. Kerrisk, *J. Appl. Phys.* **43**, 112 (1972).
- ²⁶H. J. Lee and R. E. Taylor, *J. Appl. Phys.* **47**, 148 (1976).
- ²⁷T. Y. R. Lee and R. E. Taylor, *J. Heat Transfer* **100**, 720 (1978).
- ²⁸R. D. Cowan, *J. Appl. Phys.* **32**, 1363 (1961).
- ²⁹R. D. Cowan, *J. Appl. Phys.* **34**, 926 (1963).
- ³⁰L. M. Clark III and R. E. Taylor, *J. Appl. Phys.* **46**, 714 (1975).
- ³¹H. Wang, W. D. Porter, H. Böttner, J. König, L. Chen, S. Bai, T. M. Tritt, A. Mayolet, J. Senawiratne, C. Smith, F. Harris, P. Gilbert, J. Sharp, J. Lo, H. Kleinke, and L. Kiss, *J. Electron. Mater.* **42**, 1073 (2013).
- ³²ASTM E1269-11, *Standard Test Method for Determining Specific Heat Capacity by Differential Scanning Calorimetry* (ASTM International, West Conshohocken, PA, USA, 2011).
- ³³E. Verdonck, K. Schaap, and L. C. Thomas, *Int. J. Pharm.* **192**, 3 (1999).
- ³⁴ASTM E2716-09, *Standard Test Method for Determining Specific Heat Capacity by Sinusoidal Modulated Temperature Differential Scanning Calorimetry* (ASTM International, West Conshohocken, PA, USA, 2014).
- ³⁵C. Song, P. Wang, and H. A. Makse, *Nature* **453**, 629 (2008).
- ³⁶R. Holm, *Electric Contacts: Theory and Application*, 4th ed. (Springer-Verlag, Berlin/Heidelberg/New York, 1967).
- ³⁷C. T. Moynihan, A. J. Easteal, J. Wilder, and J. Tucker, *J. Phys. Chem.* **78**, 2673 (1974).
- ³⁸J. R. Taylor, *An Introduction to Error Analysis: The Study of Uncertainty in Physical Measurements*, 2nd ed. (University Science Books, Sausalito, CA, USA, 1997).